

HYDROSTATIC EXPANSION AND SPIN CHANGES DURING TYPE I X-RAY BURSTS

ANDREW CUMMING, SHARON M. MORSINK¹, LARS BILDSTEN², JOHN L. FRIEDMAN³, & DANIEL E. HOLZ
Institute for Theoretical Physics, Kohn Hall, University of California, Santa Barbara, CA 93106

Submitted to The Astrophysical Journal

ABSTRACT

We present calculations of the spin-down of a neutron star atmosphere due to hydrostatic expansion during a Type I X-ray burst. We show that Cumming & Bildsten incorrectly calculated the change in the moment of inertia of the atmosphere during a Type I burst, resulting in a factor of two overestimation of the magnitude of the spin-down for rigidly rotating atmospheres. We derive the angular momentum conservation law in general relativity, both analytically for the case of slow rotation, and numerically for rapidly-rotating stars. We show that contrary to the claims of Heyl, but in agreement with Abramowicz and coworkers, general relativity has a small effect on the angular momentum conservation law, at the level of 5–10%. We show how to rescale our fiducial results to different neutron star masses, rotation rates and equations of state, and present some detailed rotational profiles. Comparing our results with recent observations of large frequency shifts in MXB 1658-298 and 4U 1916-053, we find that the spin-down expected if the atmosphere rotates rigidly is a factor of two to three less than the observed values. If differential rotation is allowed to persist, we find that the upper layers of the atmosphere do spin down by an amount comparable to or greater than the observed values. However, there is no compelling reason to expect the observed spin frequency to be that of only the outermost layers of the atmosphere. We conclude that hydrostatic expansion and angular momentum conservation alone cannot account for the largest frequency shifts observed during Type I bursts.

Subject headings: accretion, accretion disks — nuclear reactions — relativity — stars: neutron — stars: rotation — X-rays: bursts

1. INTRODUCTION

Type I X-ray bursts are thermonuclear flashes on the surface of weakly-magnetic ($B \lesssim 10^{10}$ G) accreting neutron stars in low mass X-ray binaries (LMXBs) (Lewin, van Paradijs, & Taam 1995; Bildsten 1998). Observations with the Rossi X-ray Timing Explorer (RXTE) have revealed nearly-coherent oscillations during Type I X-ray bursts from ten LMXBs, with frequencies in the range 270–620 Hz (for reviews, see van der Klis 2000; Strohmayer 2001). These oscillations are interpreted as rotational modulation of surface brightness asymmetries, thus providing a direct measurement of the neutron star spin frequency (Strohmayer et al. 1996). The inferred rotation periods of a few milliseconds support the idea that the neutron stars in LMXBs are the progenitors of the millisecond radio pulsars (see Bhattacharya 1995 for a review).

The large modulation amplitudes, high coherence, and frequency stability provide convincing evidence that the burst oscillation frequency is related to the neutron star spin frequency (Strohmayer 2001 and references therein). However, many puzzles remain. Open questions include (i) the origin of the asymmetry on the surface of the neutron star, particularly during the fading tail of the burst, when the burning is thought to have spread over the whole surface; (ii) why oscillations are seen in some bursts but not others, and in some sources but not others (e.g., Munro et al. 2001); and (iii) whether the oscillation frequency is the spin frequency or twice the spin frequency, motivated by comparisons of the burst oscillation frequency to the difference between the frequencies of the kHz quasi-periodic oscillations (QPOs) seen in the persistent emission (van der

Klis 2000).

The oscillation frequency increases by a few Hz during the burst. To explain this, Strohmayer et al. (1997) proposed that the burning shell decouples from the neutron star, and undergoes spin changes due to angular momentum conservation as it expands and contracts. Cumming & Bildsten (2000, hereafter CB) studied the rotational evolution of the neutron star atmosphere during a burst. Rather than addressing the complex problems of how the burning front spreads over the neutron star surface during the burst rise, or what causes the asymmetry at late times, CB asked what could be learned from detailed models of the vertical structure of the atmosphere. They computed the vertical hydrostatic expansion during the burst, and the resulting spin changes. They noted that to see a single, coherent frequency requires either the atmosphere be rigidly rotating, or the burning region to be vertically thin, so that the differential rotation across it is small (see also Miller 2000). In order to compare the theoretical results with observations, CB assumed that the burning shell rotates rigidly. They found rough agreement between the calculated spin down and observed values.

The composition of the burning shell affects the amount of expansion. For accretion rates relevant to X-ray bursters, the accreted hydrogen (H) burns via the hot CNO cycle as matter accumulates on the neutron star surface. The thermally unstable helium (He) burning which leads to the Type I X-ray burst may occur either before or after the hydrogen has been consumed (see Bildsten 1998 for a review), leading to either mixed hydrogen/helium or pure helium ignitions. The presence of a substantial amount of hydrogen leads to a factor of two greater expansion because of the lower mean molecular weight

¹Permanent address: Department of Physics, University of Alberta, Edmonton, AB, T6G 2J1, Canada

²Department of Physics, University of California, Santa Barbara, CA 93106

³Permanent address: Department of Physics, University of Wisconsin-Milwaukee, P.O. Box 413, Milwaukee, WI 53201

($\mu = 4/3$ for pure He; $\mu \approx 0.6$ for solar composition). CB noted that the largest frequency shifts observed (fractional frequency shifts $\Delta\nu/\nu \approx 0.8\%$) were difficult to achieve with pure He ignitions, requiring temperatures at the base of the burning shell extremely close to the limiting value from radiation pressure at the start of the burst. However, they also noted that no burst oscillations have been seen during Type I X-ray bursts with long ($\gtrsim 20$ s) cooling tails, characteristic of hydrogen burning (which is limited by beta decays during the rp process; Bildsten 1998), perhaps indicating a preponderance of He bursts amongst those which show oscillations. Thus they suggested that understanding the largest frequency shifts observed as being due to hydrostatic expansion together with rigid rotation might prove problematic.

Recently, two sources have shown extremely large frequency shifts. Wijnands, Strohmayer, & Franco (2001) found an increase of ≈ 5 Hz in the 567 Hz burst oscillation from MXB 1658-298. In addition to being a large frequency shift ($\Delta\nu/\nu \approx 0.9\%$), the spin evolution in this burst was unusual, with a rapid frequency increase occurring several seconds into the burst tail. This frequency shift is a little larger than the rigidly-rotating mixed H/He models of CB. Galloway et al. (2001) discovered a 270 Hz burst oscillation from the dipping source 4U 1916-053. During 4 seconds in the burst decay, the frequency increased by 3.6 Hz, a fractional shift of 1.3%, by far the largest fractional frequency shift observed so far. Comparing with the results of CB, Galloway et al. (2001) pointed out that the expansion implied by this frequency shift is larger than expected if the atmosphere rotates rigidly, especially given that the measured peak flux of the X-ray burst is sub-Eddington ($\approx 0.5 F_{\text{Edd}}$), and that the orbital period of this source (≈ 50 mins; Walter et al. 1982; White & Swank 1982; Grindlay et al. 1988) implies a hydrogen-poor companion (Nelson, Rappaport, & Joss 1986) and therefore a small fraction of hydrogen present at ignition.

In this paper, we present new calculations of the hydrostatic expansion and resulting spin-down of the neutron star atmosphere. In §2, we describe an error in CB’s calculation of the change in the moment of inertia of the burning shell, and show that the values of spin-down calculated by CB are a factor of two too large. Comparing the new results with observations, we show that, even when hydrogen is present at ignition, *the theoretical values of spin-down assuming rigid rotation are a factor of three less than the largest observed frequency shifts.* We then go on to consider different neutron star masses and equations of state. In §3, we derive the angular momentum conservation law in general relativity, presenting analytic results for slow rotation, and numerical calculations of rapidly-rotating stars. We compare our results with recent work by Heyl (2000) and Abramowicz, Kluzniak, & Lasota (2001). In §4, we show how to include general relativity and rapid rotation in the equations describing the structure of the atmosphere. We then rescale our fiducial results of §2 to different neutron star masses and equations of state, before presenting some detailed models and rotational profiles. We again show that the expected spin-down due to angular momentum conservation is smaller than the observed frequency drifts if the atmosphere rotates rigidly. We discuss the implications of our results in §5.

2. CALCULATION OF MOMENT OF INERTIA AND COMPARISON TO OBSERVATIONS

In this section, we first show that CB made an error of a factor of two in their calculation of the change in the moment of

inertia during a Type I X-ray burst, and then compare the new spin down calculations with observations.

Consider a spherical shell at the surface of the star. (The arguments of this section are unaffected by including the centrifugal distortion of the isobaric surfaces.) The mass of the shell is

$$M = \int dm = \int 4\pi r^2 \rho dr, \quad (1)$$

and its moment of inertia is

$$I = \frac{2}{3} \int r^2 dm = \frac{8\pi}{3} \int r^4 \rho dr, \quad (2)$$

where the factor of $2/3$ comes from integrating over angles. Following CB, we adopt a plane-parallel approximation for the thin atmosphere, and write $r = R + z$, keeping only first order terms in z/R . Changing integration variables from radius r to column depth y , where $dy = -\rho dr$, equation (2) reduces to CB’s equation (19) for the moment of inertia. If the angular momentum of the atmosphere, $I\Omega$, is conserved, the spin-down is given by comparing its moment of inertia before the burst with that during the burst, $\Delta\Omega/\Omega = -\Delta I/I$.

The error in CB’s calculation of the change in moment of inertia arises because they assume that the total column depth of the atmosphere is constant during the burst. We now show that this is not the case when the mass of the layer is conserved. We write the mass of the shell as

$$M = 4\pi R^2 \int \left[1 + \frac{2z(y)}{R} \right] dy = 4\pi R^2 \Delta y \left(1 + \frac{2\langle z \rangle}{R} \right), \quad (3)$$

where Δy is the total column depth, and we define a mass-weighted thickness $\langle z \rangle = \int z(y) dy / \Delta y$. If the vertical extent of the layer $\langle z \rangle$ changes, so must its total column depth Δy if the total mass M is conserved. Physically, a thin spherical shell has a greater surface area if it moves radially outwards, and so must have a lower column depth in order to conserve its total mass. By taking the column depth at the base during the burst to be the same as that before the burst, CB unwittingly increased the mass of the layer during the burst, and so overestimated the change in its moment of inertia.

Rather than including the change in the column depth of the layer explicitly, we write the mass element in equation (2) as $dm = 4\pi R^2 dy$, so that there is a unique correspondence between mass and column depth. The moment of inertia is then

$$I = \frac{8\pi R^4}{3} \int_{y_t}^{y_b} \left[1 + \frac{2z(y)}{R} \right] dy, \quad (4)$$

where the integration limits are now held fixed during the burst, thereby keeping the mass of the layer constant, $M = 4\pi R^2 \Delta y = 4\pi R^2 (y_b - y_t)$. We have checked the validity of this expression by integrating the full spherical equations for this problem. In this paper, we adopt a plane-parallel approximation because it allows us to straightforwardly incorporate the general relativistic angular momentum conservation law.

The spin changes during the burst result from changes in the vertical extent of the atmosphere, which are described by the second term of equation (4). Equation (19) of CB has a factor $4z/R$ rather than $2z/R$, so that the spin-down calculated by CB is too large by a factor of 2. Specifically, both the spin-down of the convection zone shown in Figures 2 and 6 of CB, and the spin-down of a rigidly-rotating atmosphere shown in Figure 13

of CB, should be reduced by a factor of 2. The spin-down of the radiative layers shown in Figures 2, 4 and 6 of CB is, however, calculated correctly, since in that case CB assumed $r^2\Omega$ was constant for each spherical shell.

Figure 1 shows the spin-down calculated using equation (4) for the moment of inertia, presuming the whole atmosphere rotates rigidly during the burst. This is an updated version of Figure 13 of CB, and detailed discussion of the theoretical models may be found in that paper. The calculated spin down is exactly a factor of two less than found by CB. We take $g = 1.9 \times 10^{14} \text{ cm s}^{-2}$, the Newtonian gravity for a $1.4 M_\odot$, 10 km star. We consider two pre-burst models, mixed H/He ignition at $\dot{m} = 0.1 \dot{m}_{\text{Edd}}$ (solid lines and squares), and pure He ignition at $\dot{m} = 0.015 \dot{m}_{\text{Edd}}$ (dotted lines and open squares).

Figure 1 shows results for both convective and radiative models. For the radiative models, we show the spin down as a function of flux, since the radiative solution is uniquely determined by the flux. The convective models depend both on the flux and the extent of the convection zone; we plot the spin down resulting from the convective models given in Table 3 of CB. The convective models have a composition profile the same as that prior to the burst. The radiative models have either a pre-burst composition (upper solid and dotted curves) or a composition of heavy elements (lower solid and dotted curves), either ^{56}Ni for pure He burning, or ^{76}Kr for mixed H/He burning (we choose ^{76}Kr as representative of the products of rp process H burning; see Schatz et al. 1998; Koike et al. 1999; Schatz et al. 2001). As described in CB, the radiative and convective models with a pre-burst composition are appropriate for the burst rise, whereas the radiative atmospheres composed of heavy elements are appropriate for the cooling tail of bursts. Convective models spin down more than radiative models because the steeper temperature gradient in the convection zone leads to a larger base temperature for a given flux.

On the left of Figure 1, we plot the observed frequency drifts as horizontal bars. A summary of these observations may be found in CB, Table 1; in addition, we include the frequency shifts recently reported for 4U 1916-053 (Galloway et al. 2001) and MXB 1658-298 (Wijnands et al. 2001). For each source, we plot the largest observed frequency shift. We plot as upper limits those cases for which a frequency was only seen in the burst tail. The largest observed frequency shift is larger than the theoretical values by at least a factor of 3.

3. ANGULAR MOMENTUM CONSERVATION IN GENERAL RELATIVITY

In this section, we derive the angular momentum conservation law in general relativity. Our approach is to calculate the conserved angular momentum of a particle moving on a circular path (in the Appendix, we show that the same result is obtained starting with the conservation equations for a fluid). We show analytic results for slowly rotating stars, and present numerical calculations of rapidly rotating stars. We compare our results with recent calculations by Heyl (2000) and Abramowicz et al. (2001).

In Newtonian physics, the specific angular momentum of a particle is given by $r^2\Omega$, where r is the distance from the rotation axis. If the particle's motion conserves angular momentum, the change in its spin frequency with radius is given by $d \ln \Omega / d \ln r = -2$. In this section, we derive the equivalent expression in general relativity. We start by discussing the angular momentum of a particle moving in the Schwarzschild metric. We then derive the conserved angular momentum in the slow

rotation approximation, i.e. neglecting terms of order $(\Omega/\Omega_K)^2$, where $\Omega_K^2 = GM/R^3$, allowing us to write an analytic expression for the angular momentum conservation law. However, since $(\Omega/\Omega_K)^2$ may be quite large (for example, $(\Omega/\Omega_K)^2 = 0.26$ for a star with $R = 15 \text{ km}$ and $M = 1.4 M_\odot$ spinning at 600 Hz), we conclude this section with detailed numerical calculations of rapidly rotating models.

Consider first a spherical star, for which the metric is

$$ds^2 = -e^\nu dt^2 + e^\lambda dr^2 + r^2 (d\theta^2 + \sin^2 \theta d\phi^2), \quad (5)$$

where outside the star the metric functions λ and ν are given by

$$e^\nu = e^{-\lambda} = 1 - \frac{2M}{r} \quad (6)$$

where M is the total gravitational mass. Note that in this paper we write the ratio GM/rc^2 as M/r for clarity, but otherwise explicitly write in the constants G and c . A particle moving in a circular path has four-velocity (e.g., Hartle 1970)

$$u^\alpha = u^t (t^\alpha + \Omega(r)\phi^\alpha), \quad (7)$$

where $\Omega(r)$ is the angular velocity measured by an observer at infinity, u^t is the redshift factor between the particle and the observer at infinity, and t^α and ϕ^α are Killing vectors of the spacetime. The redshift factor is

$$u^t = e^{-\nu/2} = \left(1 - \frac{2M}{r}\right)^{-1/2}, \quad (8)$$

where we choose the standard normalization $g_{\alpha\beta}u^\alpha u^\beta = -1$. Associated with the Killing vectors t^α and ϕ^α are the conserved quantities $E = -u^\alpha t_\alpha$ and $L = u^\alpha \phi_\alpha$, the specific energy and angular momentum. Using equations (7) and (8), we obtain (see, e.g. Schutz 1990, §7.4)

$$E = \left(1 - \frac{2M}{r}\right)^{1/2}, \quad (9)$$

and

$$L = r^2 \sin^2 \theta \Omega \left(1 - \frac{2M}{r}\right)^{-1/2}. \quad (10)$$

Differentiating equation (10) and evaluating it at the surface of the star, we find

$$\frac{d \ln \Omega}{d \ln r} = -2 \left(1 - \frac{5M}{2R}\right) \left(1 - \frac{2M}{R}\right)^{-1} \quad (11)$$

when a particle moves such that angular momentum is conserved. In the limit $M \ll R$, this formula reduces to the Newtonian result.

It is simple to extend this analysis to the case of slow rotation, for which the metric is (Hartle 1967)

$$ds^2 = -e^\nu dt^2 + e^\lambda dr^2 + r^2 (d\theta^2 + \sin^2 \theta d\phi^2) - 2\omega r^2 \sin^2 \theta d\phi dt, \quad (12)$$

where λ and ν have the same solutions as the spherical case outside the star, and where $\omega = 2J/r^3$ outside the star (J is the total angular momentum of the star). Again solving for the conserved angular momentum, we find

$$L = r^2 \sin^2 \theta (\Omega - \omega) \left(1 - \frac{2M}{r}\right)^{-1/2}, \quad (13)$$

giving

$$\frac{d \ln \Omega}{d \ln r} = -2 \left[1 - \frac{5M}{2R} + \frac{I}{R^3} \left(1 - \frac{M}{R} \right) \right] \left(1 - \frac{2M}{R} \right)^{-1}, \quad (14)$$

at the surface of the star, where we presume the particle is initially rotating with the spin of the star, and write the moment of inertia $I = J/\Omega$.

For the rapidly-rotating case, we consider the general metric for an axisymmetric stationary star,

$$ds^2 = -e^{\gamma+\rho} dt^2 + e^{\gamma-\rho} \bar{r}^2 \sin^2 \theta (d\phi - \omega dt)^2 + e^{2\alpha} (d\bar{r}^2 + \bar{r}^2 d\theta^2), \quad (15)$$

where the metric potentials ρ, γ, α and ω depend only on the coordinates \bar{r} and θ . The coordinate \bar{r} is related to the Schwarzschild coordinate r by $r = \bar{r} \exp(\frac{1}{2}(\gamma - \rho))$, so that $2\pi \bar{r} \sin \theta$ is the circumference of a circle with constant \bar{r} and θ . For further details about the interpretation of these coordinates and potentials, see Friedman, Ipser & Parker (1986) and Morsink & Stella (1999). Given an equation of state, a mass and a rotation rate, the metric (15) can be solved numerically. We use a code written by N. Stergioulas⁴, which assumes rigid rotation and is based on methods developed by Komatsu, Eriguchi & Hachisu (1989) and Cook, Shapiro & Teukolsky (1994).

We present the properties of some rapidly-rotating models in Table 1. We consider two different equations of state (EOS), EOS L which is stiff and EOS APR which is softer. EOS L (Pandharipande & Smith 1975) is one of the stiffest EOS in the Arnett & Bowers (1977) catalogue. EOS APR is the model A18+ $\delta\nu$ +UIX* computed by Akmal, Pandharipande & Ravenhall (1998) which uses modern nucleon scattering data and first order special relativistic corrections. For each EOS, we consider two different masses, $M = 1.4 M_\odot$ and $2.0 M_\odot$, and two spin frequencies, $\nu = 300$ Hz and 600 Hz. The last column in Table 1 gives the break-up spin frequency in each case.

We work in the equatorial plane, and do not consider the variations of the metric potentials with latitude. The specific angular momentum is

$$L = \frac{vr}{\sqrt{1-\nu^2}}, \quad (16)$$

(see also Morsink & Stella 1999) where the three-velocity of a corotating particle as measured by a zero angular momentum observer is given by

$$v = r e^{-(\gamma+\rho)/2} [\Omega(r) - \omega(r)]. \quad (17)$$

Again holding L constant as we vary the Schwarzschild coordinate radius r , we find

$$\frac{d \ln \Omega}{d \ln r} = -2 \left[\left(1 - \frac{v^2}{2} - \frac{R}{4} (\gamma_r + \rho_r) \right) \left(1 - \frac{\omega}{\Omega} \right) - \frac{R}{2\Omega} \omega_r \right], \quad (18)$$

where R is the equatorial radius of the star, subscripts denote partial differentiation and all quantities are evaluated at the equator. In the slow rotation limit, equations (16) and (18) reduce to equations (13) and (14).

Heyl (2000) recently calculated $d \ln \Omega / d \ln r$, with a rather different result (compare our eq. [14] with his eq. [10]). However, Abramowicz et al. (2001) point out a sign error in Heyl's calculation, and, more importantly, that Heyl assumes that the quantity L/E is conserved, as, for example, a particle in orbit (Abramowicz & Prasanna 1990). However, the energy E of

a fluid element in the atmosphere is not conserved during the burst. The correct conserved quantity, which we have considered in this section, is the angular momentum per particle L . In the slow rotation approximation, our result (eq. [14]) agrees with equation (9) of Abramowicz et al. (2001).

We write $d \ln \Omega / d \ln r$ as -2β , where

$$\beta \equiv -\frac{1}{2} \frac{d \ln \Omega}{d \ln r} \quad (19)$$

is unity in the Newtonian limit. We give the value of β in Table 1. Figure 2 shows β as a function of neutron star mass for EOS APR and EOS L, and for $\nu = 300$ and 600 Hz. We see that including the general relativistic angular momentum conservation law changes $d \ln \Omega / d \ln r$ by 5–10%.

4. CALCULATION OF EXPANSION AND SPIN DOWN

In this section, we present calculations of the expansion and spin-down of the atmosphere, including the effects of general relativity and rapid rotation. In the spirit of CB, we ignore latitudinal variations, and work in the equatorial plane. First, in §4.1, we discuss the effects of general relativity on the equations describing the hydrostatic and thermal structure of the atmosphere, and calculate the reduction in gravity at the equator due to rapid rotation. In §4.2, we show how to include the general relativistic angular momentum conservation law that we obtained in §3. In §4.3, we rescale our fiducial results of §2 for the spin-down of a rigidly-rotating atmosphere to different masses, equations of state, and spin frequencies. In §4.4, we relax the assumption of rigid-rotation, and present the rotational profiles of the atmosphere for several different cases.

4.1. Hydrostatic and Thermal Structure of the Atmosphere

We now write down the differential equations describing the hydrostatic and thermal structure of the atmosphere including general relativity, and compare them to the Newtonian equations. We start by considering a non-rotating star, and then discuss the additional effects of rotation.

For a spherical star, Thorne (1977) (see also Thorne 1967) gives the equation for mass conservation as

$$\frac{dM_r}{dr} = 4\pi r^2 \rho \mathcal{V}(r), \quad (20)$$

where M_r is the rest mass (number of baryons multiplied by baryon rest mass) within coordinate radius r , ρ is the rest mass density, and \mathcal{V} is the ‘‘volume redshift factor’’. For slow rotation, $\mathcal{V}(r) = (1 - 2M(r)/r)^{-1/2}$, where $M(r)$ is the gravitational mass interior to r . We adopt a plane parallel approximation in the thin envelope, and write $r = R + z/\mathcal{V}$, where $z \ll R$ is the proper length. Here, \mathcal{V} is the redshift factor at the surface of the star $\mathcal{V} = \mathcal{V}(R)$. We define the rest mass column depth $dy = -dM_r / 4\pi R^2$. The mass conservation equation becomes

$$\frac{dz}{dy} = -\frac{1}{\rho}. \quad (21)$$

The equation for hydrostatic balance is (Thorne 1977)

$$\frac{dP}{dM_r} = -\frac{GM(r)}{4\pi r^4} \mathcal{V}, \quad (22)$$

⁴Code publicly available at <http://www.gravity.phys.uwm.edu/rns/>

where P is the locally measured pressure, and we neglect contributions to the gravitational mass from the fluid energy density. Using the definition of column depth, we rewrite equation (22) for the thin layer as

$$\frac{dP}{dy} = g, \quad (23)$$

where

$$g = \frac{GM}{R^2} \mathcal{V}. \quad (24)$$

Rewriting the entropy and flux equations (Thorne 1977, eqs. [11d] and [11h]) in a similar way, we find

$$\frac{dF}{dy} = -\epsilon \quad (25)$$

and

$$\frac{dT}{dy} = \frac{3\kappa}{4acT^3} F, \quad (26)$$

where F is the heat flux, ϵ is the nuclear energy release rate per unit rest mass, κ is the opacity, and T is the locally measured temperature. Equations (21), (23), (25), and (26), which describe the structure of the atmosphere, are identical to the Newtonian equations (compare CB §2).

These results also hold in the slow rotation approximation, for which the star is spherical to first order in $(\Omega/\Omega_K)^2$. The inclusion of rapid rotation has three effects. The first is to change the volume correction factor \mathcal{V} . In addition, the mass conservation equation must be covariant so that all observers agree on the rest mass of the star. This requirement gives an additional Lorentz factor in equation (20) (e.g., Friedman et al. 1986). However, we find that for the models we consider in this paper, both of these effects are $\lesssim 1\%$, and so we neglect them.

Much more important is the correction to gravity due to the rapid rotation. This correction factor is the relativistic generalisation of the Newtonian reduction in gravitational acceleration due to the centrifugal force. To calculate this, we write the four-velocity as $u^\alpha = \mathcal{R}(t^\alpha + \Omega\phi^\alpha)$, and use the normalization $u^\alpha u_\alpha = -1$ to solve for the redshift factor

$$\mathcal{R} = e^{-(\gamma+\rho)/2} \frac{1}{\sqrt{1-v^2}}, \quad (27)$$

where v is given by equation (17). The equation of hydrostatic balance for a rigidly rotating star is then (Friedman et al 1986)

$$\frac{1}{\rho} \frac{dP}{dr} = -\frac{d}{dr} \log \mathcal{R}, \quad (28)$$

where we assume the pressure is much smaller than the rest mass density. To reduce this equation to the form of equation (23), we write

$$g = \frac{GM}{R^2} \mathcal{V} \mathcal{A}, \quad (29)$$

where the correction factor \mathcal{A} accounts for the reduction in g at the equator due to rapid rotation,

$$\mathcal{A} = \frac{R^2}{GM\mathcal{V}^2} \frac{d}{dr} \log \mathcal{R}, \quad (30)$$

tending to unity in the limit of zero rotation. This is the most important effect coming from rotation, giving a correction of up to 25% for a rotation frequency of 600 Hz and a stiff equation of state.

In summary, the general relativistic equations look the same as the Newtonian equations if we use the correct value of surface gravity g (eq. [29]), and if we identify the column depth y with the rest mass column depth, and the thickness z with the proper thickness of the layer. Values of g , \mathcal{V} , and \mathcal{A} are given in Table 1 for different models.

4.2. Calculation of Spin Down

To incorporate the general relativistic angular momentum conservation law into our calculations of spin down, we write the angular momentum per unit rest mass at the equator in the form

$$u_\phi = \Omega f(r), \quad (31)$$

where $f(r)$ is a function of radius, e.g. $f(r) = r^2$ in the Newtonian limit. If the angular momentum is constant, we find that the change of Ω with radius is determined by the gradient of f with radius: $\beta = (-1/2)(d \ln \Omega / d \ln r) = (1/2)(d \ln f / d \ln r)$. Now consider a particle which moves from radius R to $R + \Delta r$, where $\Delta r \ll R$. Conservation of angular momentum gives $u_\phi(R + \Delta r) = u_\phi(R)$. Expanding in a Taylor series around $r = R$, we find

$$\frac{\Delta \Omega}{\Omega} = -\beta \left(\frac{2\Delta r}{R} \right). \quad (32)$$

In the Newtonian limit, for which $\beta = 1$, we recover the familiar result $\Delta \Omega / \Omega = -2\Delta r / R$. To calculate the moment of inertia, we must modify equation (4). Again writing the angular momentum in the form of equation (31), and expanding $f(r)$ around $r = R$, we find

$$I = \frac{8\pi R^2 f(R)}{3} \int \left[1 + \frac{2\beta z(y)}{\mathcal{V}R} \right] dy, \quad (33)$$

which reduces to equation (4) in the Newtonian limit.

4.3. Scaling our Fiducial Results to Different Masses and Equations of State

The calculations presented in §2 were for a surface gravity $g = 1.9 \times 10^{14} \text{ cm s}^{-2}$ (the Newtonian gravity for a $1.4M_\odot$, $R = 10 \text{ km}$ neutron star). We now rescale these fiducial results to different masses and equations of state, including the effects of rapid rotation and general relativity.

To calculate the thickness of the atmosphere in §2, we integrated hydrostatic balance in the form $dP/dz = -\rho GM/R^2$, giving the thickness $\Delta z/R \propto 1/gR \propto R/M$ (see also §2 of CB). In addition, we must include a factor \mathcal{V} to obtain the correct general relativistic value for g , and a factor \mathcal{A} to include the effects of rotation on gravity. We thus find the fractional change in thickness of the atmosphere is

$$\frac{\Delta z}{R} = \mathcal{V}^{-1} \mathcal{A}^{-1} \left(\frac{0.21}{M/R} \right) \left(\frac{\Delta z}{R} \right)_0, \quad (34)$$

where $(\Delta z/R)_0$ is the fiducial value from §2. The fractional change in spin frequency is $\beta(2\Delta r/R)$, where Δr is the coordinate thickness. Converting to proper thickness Δz involves another factor of \mathcal{V} , giving

$$\frac{\Delta \Omega}{\Omega} = \beta \mathcal{V}^{-2} \mathcal{A}^{-1} \left(\frac{0.21}{M/R} \right) \left(\frac{\Delta \Omega}{\Omega} \right)_0 \equiv \alpha \left(\frac{\Delta \Omega}{\Omega} \right)_0, \quad (35)$$

where we define α as the scaling factor from the fiducial value, and we took $M/R = 0.21$ in §2. Note that the largest contributions to α come from rescaling gravity and including the centrifugal force, rather than from general relativistic effects.

Figure 3 shows α as a function of neutron star mass, for EOS APR and EOS L, and in each case for $\nu = 300$ and 600 Hz. We also give α in Table 1. Figure 3 shows that for massive neutron stars with $M \approx 2M_\odot$, the frequency shifts calculated in §2 and shown in Figure 1 should be multiplied by 0.65–0.85 for EOS L, and 0.3–0.4 for EOS APR. For a $1.4M_\odot$ star, these factors are 1.1–1.7 for EOS L, and 0.7–0.8 for EOS APR. The largest values of α are obtained for a low neutron star mass, stiff equation of state, and rapid rotation. However, even $\alpha = 1.7$ for $M = 1.4 M_\odot$, EOS L, and $\nu = 600$ Hz is not large enough to give agreement with the largest observed frequency shifts.

4.4. Rotational Profiles

In Figure 4, we present some rotational profiles for some specific models. We take the neutron star mass to be $1.4 M_\odot$, the global accretion rate to be $0.1 \dot{M}_{\text{Edd}}$, and again work in the equatorial plane. We assume that the atmosphere is rigidly-rotating immediately prior to the burst, and that during the burst, the atmosphere is radiative and carries a flux equal to the solar-composition Eddington flux at the photosphere ($F_{\text{Edd}} = 8.8 \times 10^{24} g_{14} \text{ erg cm}^{-2} \text{ s}^{-1}$). For $\nu = 300$ and $\nu = 600$ Hz, and for EOS L and EOS APR, we plot the rotational profiles assuming either (i) complete rotational coupling, resulting in rigid rotation across the layer, or (ii) no angular momentum transport, giving a differentially-rotating layer.

If we allow differential rotation to persist, we see that the upper layers of the atmosphere spin down by an amount comparable to or greater than the observed spin changes during bursts. However, it is not clear why the spin frequency observed should be that of only the outermost layers. Indeed, CB (§3.4) argued that substantial differential rotation would wash out any signal from the deeper cooling layers because of the finite time to transport heat vertically.

5. SUMMARY AND DISCUSSION

We have presented new calculations of the hydrostatic expansion and spin-down of a neutron star atmosphere during a Type I X-ray burst. Our main conclusion is that hydrostatic expansion is not enough to explain the observed frequency drifts during Type I X-ray bursts if the burning atmosphere rotates rigidly.

In §2, we showed that Cumming & Bildsten (2000) (CB) overestimated the change in the moment of inertia of the atmosphere, obtaining values of spin-down that were a factor of two too large. Figure 1 compares the new calculations of spin-down with observations, including recent measurements of large frequency drifts during bursts (Galloway et al. 2000; Wijnands et al. 2001). We find that the largest observed frequency shift is a factor of 3 or more greater than the theoretical values.

In §3, we derived the angular momentum conservation law in general relativity. We calculated the variation of spin frequency with radial distance, $d \ln \Omega / d \ln r$, for a particle moving with constant angular momentum. In the slow rotation approximation ($\Omega^2 \ll GM/R^3$), we obtained the analytic result given by equation (14), which agrees with recent work by Abramowicz et al. (2001). For rapidly-rotating stars, we calculated $d \ln \Omega / d \ln r$ by numerically solving for the structure of the neutron star. The correction to the Newtonian angular momentum conservation law, $\beta = (-1/2)(d \ln \Omega / d \ln r)$, is shown in

Figure 2 for different neutron star masses, equations of state and spin frequencies. Contrary to the results of Heyl (2000), which were also shown to be incorrect by Abramowicz et al. (2001), we find that the general relativistic correction is small, about 5–10%.

In §4, we calculated the atmospheric expansion and spin-down, including the effects of rapid rotation and general relativity. Working in the equatorial plane (in the spirit of CB’s calculation, we neglect latitudinal variations in this paper), we calculated the scaling factor α required to rescale our fiducial results of §2 to different neutron star masses, equations of state, and spin frequencies (Figure 3). In addition, we presented the rotational profiles for some particular models (Figure 4). We find that the largest spin-down is for rapid rotation, and low mass stars with a stiff equation of state. For example, a $1.4 M_\odot$ star spinning at 600 Hz with the stiff equation of state EOS L has $\alpha = 1.7$. However, this is not a large enough factor to bring observations and theory into agreement in Figure 1.

The rotational profiles given in Figure 4 show that in principle frequency shifts as large as those observed can be obtained by hydrostatic expansion, if we consider only the outermost layers of the atmosphere, and allow differential rotation. However, it is not at all obvious why the observed frequency would be that of the outermost shells of the atmosphere, which contain a small amount of the mass, particularly since the energy release is in the deeper layers. Indeed, CB argued (see their §3.4) that substantial differential rotation in the burning layers would wash out the signal, because of the finite time needed to transport heat vertically in the atmosphere.

Another possible objection to the angular momentum conservation picture was given by CB, who pointed out that if the burning layers are threaded by a large scale poloidal magnetic field, this field will be wound up by the differential rotation during the burst. The wound up toroidal field acts back on the shear, halting and reversing its direction in the time for an Alfvén wave to cross the atmosphere (see, for example, Spruit 1999). For a magnetic field typical of a millisecond radio pulsar, $B \sim 10^8$ G, this timescale is only ~ 0.01 s. One possibility is that the surface field is much weaker, $B \lesssim 10^6$ G, allowing shearing to persist. Observations of burst oscillations in the accreting millisecond X-ray pulsar SAX J1808.4-3658, which perhaps has a $\sim 10^8$ – 10^9 G field (Psaltis & Chakrabarty 1999), would give an interesting test of this picture. In’t Zand et al. (2000) report a marginal detection with BeppoSAX of oscillations at 400 ± 2 Hz during a Type I burst, but are unable to resolve any frequency drift. Unfortunately, as yet no burst oscillations have been detected from this source with RXTE.

The results we have obtained in this paper suggest that we may have to look elsewhere for an explanation of the frequency drifts. Spitkovsky, Levin, & Ushomirsky (2001), in a detailed investigation of hydrodynamic flows during Type I bursts, propose that the frequency drifts may be explained by a combination of radial expansion and variations in the velocity of zonal flows on the neutron star surface. Another possibility mentioned by CB is that the burst oscillation is due to a non-radial oscillation in the neutron star surface layers. Such possibilities remain to be investigated in detail.

We thank Jeremy Heyl and Scott Hughes for many useful discussions, and Yuri Levin for a careful reading of the manuscript. We are grateful to Chris Matzner for insights into the issues discussed in the Appendix. This work began at the program on

Spin and Magnetism in Young Neutron Stars, ITP, Santa Barbara. A. C. and S. M. thank the Canadian Institute for Theoretical Astrophysics for hospitality during its completion. This research was supported by the National Science Foundation un-

der grants PHY99-07949 and AY97-31632, by NASA via grant NAG 5-8658, and by the Natural Sciences and Engineering Research Council of Canada. L. B. is a Cottrell Scholar of the Research Corporation.

REFERENCES

- Abramowicz, M. A., Kluzniak, W., & Lasota, J.-P. 2001, *A&A*, 374, L16
 Abramowicz, M. A., & Prasanna, A. R. 1990, *MNRAS*, 245, 720
 Akmal, A., Pandharipande, V. R., & Ravenhall, D. G. 1998, *Phys. Rev. C*, 58, 1804
 Arnett, W. D., & Bowers, R. L. 1977, *ApJS*, 33, 415
 Bhattacharya, D. 1995, in *X-Ray Binaries*, ed. W. H. G. Lewin, J. van Paradijs, & E. P. J. van den Heuvel (Cambridge: Cambridge University Press), 233
 Bildsten, L., 1998, in *The Many Faces of Neutron Stars*, ed. R. Buccheri, J. van Paradijs, & M. A. Alpar (Dordrecht:Kluwer), 419
 Cook, G. B., Shapiro, S. L., & Teukolsky S. A. 1994, *ApJ*, 424, 823
 Cumming, A., & Bildsten, L. 2000, *ApJ*, 544, 453 (CB)
 Friedman, J.L., Ipser, J.R., & Parker, L. 1986, *ApJ*, 304, 115
 Galloway, D. K., Chakrabarty, D., Muno, M. P., & Savov, P. 2001, *ApJ*, 549, L85
 Grindlay, J. E., Bailyn, C. D., Cohn, H., Lugger, P. M., Thorstensen, J. R., & Wegner, G. 1988, *ApJ*, 334, L25
 Hansen, C. J., & Kawaler, S. D. 1994, *Stellar Interiors: Physical Principles, Structure and Evolution* (New York: Springer-Verlag)
 Hartle, J. B. 1967, *ApJ*, 150, 1005
 Hartle, J. B. 1970, *ApJ*, 161, 111
 Heyl, J. S. 2000, *ApJ*, 542, L45
 In't Zand, J. J. M., et al. 2001, *A&A*, in press (astro-ph/0105324)
 Koike, O., Hashimoto, M., Arai, K., & Wanajo, S. 1999, *A&A*, 342, 464
 Komatsu, H., Eriguchi, Y., & Hachisu, I. 1989, *MNRAS*, 237, 355
 Lewin, W. H. G., van Paradijs, J., & Taam, R. E. 1995, in *X-Ray Binaries*, ed. W. H. G. Lewin, J. van Paradijs, & E. P. J. van den Heuvel (Cambridge: Cambridge Univ. Press), 175
 Mihalas, D., & Mihalas, B. W. 1984, *Foundations of Radiation Hydrodynamics* (Oxford: Oxford University Press)
 Miller, M. C. 2000, *ApJ*, 531, 458
 Morsink, S. M., & Stella, L. 1999, *ApJ*, 513, 827
 Muno, M. P., Chakrabarty, D., Galloway, D. K., & Savov, P. 2001, *ApJ*, 553, L157
 Nelson, L. A., Rappaport, S. A., & Joss, P. C. 1986, *ApJ*, 304, 231
 Pandharipande, V. R., & Smith, R. A. 1975, *Phys. Lett. B*, 59, 15
 Psaltis, D., & Chakrabarty, D. 1999, *ApJ*, 521, 332
 Ravenhall, D. G., & Pethick C. J. 1994, *ApJ*, 424, 846
 Schatz, H., et al. 1998, *Phys. Rep.*, 294, 167
 Schatz, H., et al. 2001, *Phys. Rev. Lett.*, 86, 3471
 Schutz, B. F. 1990, *A First Course in General Relativity* (Cambridge University Press: Cambridge)
 Spitkovsky, A., Levin, Y., & Ushomirsky, G. 2001, in preparation
 Spruit, H. C. 1999, *A&A*, 349, 189
 Strohmayer, T. 2001, astro-ph/0012516
 Strohmayer, T. E., Jahoda, K., Giles, B. A., & Lee, U. 1997, *ApJ*, 486, 355
 Strohmayer, T. E., Zhang, W., Swank, J. H., Smale, A., Titarchuk, L., Day, C., & Lee, U. 1996, *ApJ*, 469, L9
 Thorne, K. S. 1967, in *High Energy Astrophysics*, Vol. 3, ed. C. DeWitt, E. Schatzman, and P. Veron, Proc. 1966 Les Houches Summer School (New York: Gordon & Breach)
 Thorne, K. S. 1977, *ApJ*, 212, 825
 van der Klis, M. 2000, *ARA&A*, 38, 717
 Walter, F. M., Mason, K. O., Clarke, J. T., Halpern, J., Grindlay, J. E., Bowyer, S., & Henry, J. P. 1982, *ApJ*, 253, L67
 White, N. E., & Swank, J. H. 1982, *ApJ*, 253, L61
 Wijnands, R., Strohmayer, T., & Franco, L. M. 2001, *ApJ*, 549, L71

TABLE 1
NEUTRON STAR MODELS

$M (M_{\odot})$	R (km)	M/R	\mathcal{V}^a	g (10^{14} cm s $^{-2}$)	\mathcal{A}^b	β^c	α^d	ν_B^e (Hz)
EOS APR $\nu = 300$ Hz								
1.4	11.5	0.18	1.25	1.72	0.98	0.94	0.72	1070
2.0	11.1	0.27	1.46	3.10	0.99	0.90	0.34	1330
EOS APR $\nu = 600$ Hz								
1.4	11.9	0.17	1.24	1.48	0.91	0.94	0.81	1070
2.0	11.3	0.26	1.45	2.83	0.95	0.90	0.37	1330
EOS L $\nu = 300$ Hz								
1.4	15.2	0.14	1.17	0.90	0.95	0.96	1.13	730
2.0	15.3	0.19	1.28	1.39	0.97	0.94	0.65	850
EOS L $\nu = 600$ Hz								
1.4	16.7	0.12	1.15	0.55	0.72	0.95	1.70	730
2.0	16.2	0.18	1.25	1.05	0.83	0.93	0.82	850

^aThe redshift factor $\mathcal{V} = (1 - 2M/R)^{-1/2}$ (we neglect the $\lesssim 1\%$ correction due to rotation).

^bThe correction to gravity due to rapid rotation, $g = GM\mathcal{V}\mathcal{A}/R^2$.

^cThe general relativistic correction to the angular momentum conservation law, $\beta \equiv (-1/2)(d \ln \Omega / d \ln r)$.

^dThe multiplicative scaling factor that should be applied to the results of §2 and Fig. 1, to allow for the different gravity, and the effects of general relativity and rapid rotation (see text).

^eThe break-up spin frequency.

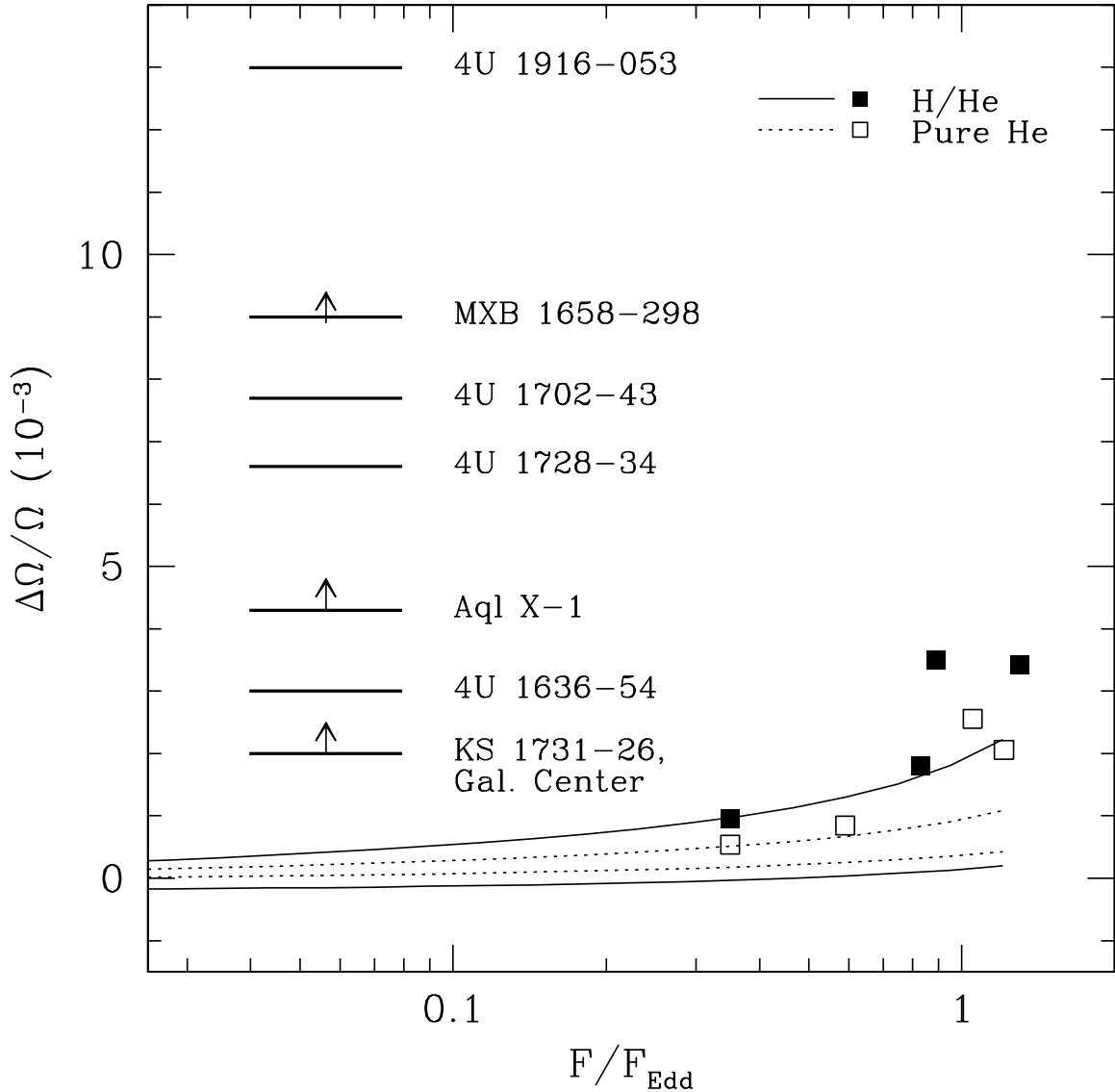


FIG. 1.— The spin evolution of the atmosphere for convective (*squares*) and radiative models (*lines*), assuming rigid rotation is maintained throughout the atmosphere. We plot the fractional spin frequency change of the burning shell, $\Delta\Omega/\Omega$, such that $\Delta\Omega/\Omega > 0$ indicates spin down. We show results for both mixed H/He ignitions (*solid lines, solid squares*) and pure He ignitions (*dotted lines, open squares*). For the convective models, the composition is the same as before ignition. For the radiative models, the upper curve is for a pre-burst composition; the lower curve is for a composition of ^{56}Ni (pure He) or ^{76}Kr (mixed H/He). We indicate the observed frequency shifts by horizontal bars. These observations are summarized in Table 1 of CB; in addition, we include the frequency shifts recently reported for 4U 1916-053 (Galloway et al. 2001) and MXB 1658-298 (Wijnands et al. 2001). For those bursts in which the oscillation frequency was seen only in the tail, we plot the $\Delta\Omega/\Omega$ value as a lower limit. This Figure is an update of Figure 13 of CB.

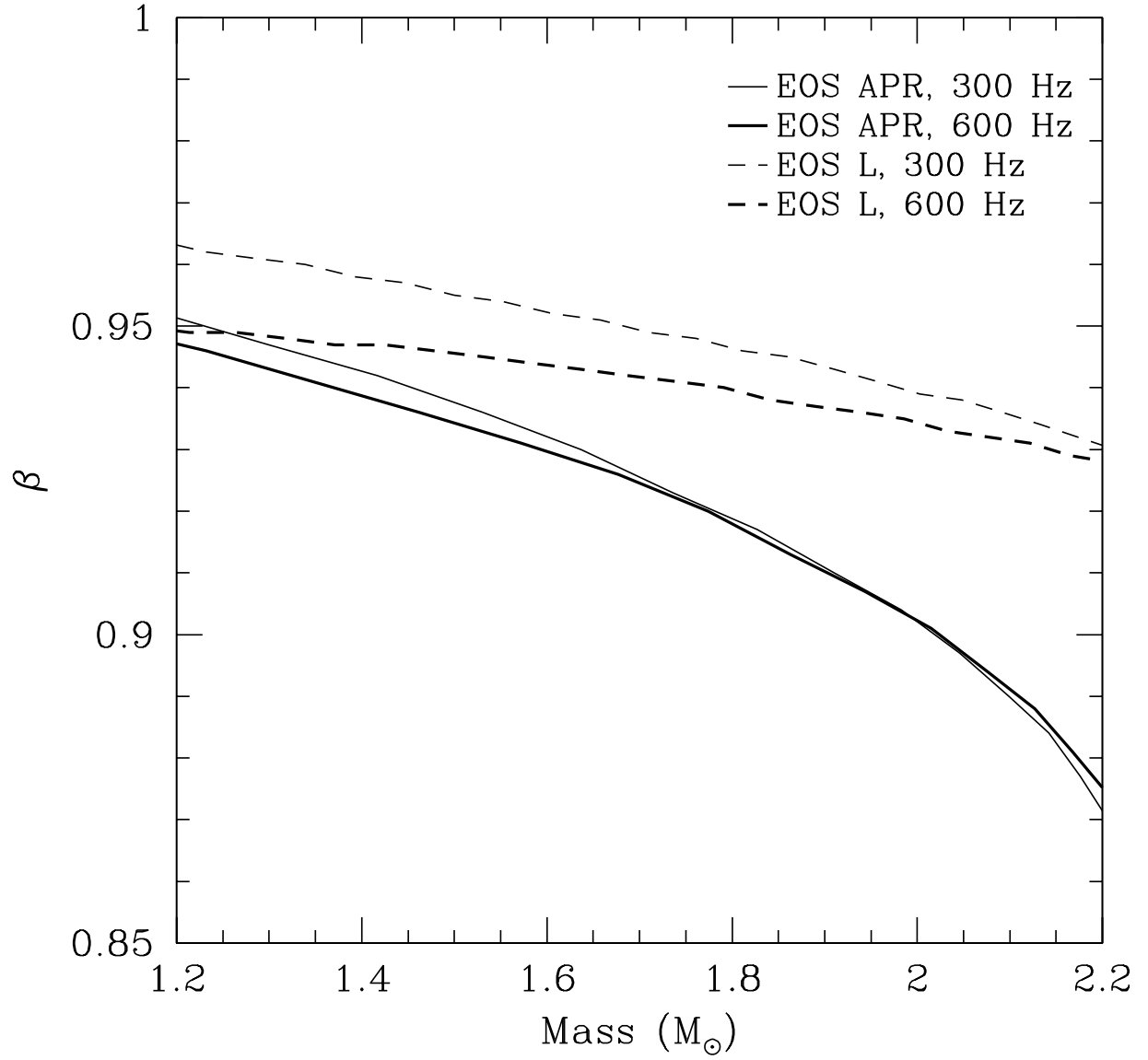


FIG. 2.— The general relativistic correction to the Newtonian angular momentum conservation law. We plot $\beta = (-1/2)(d \ln \Omega / d \ln r)$ as a function of neutron star mass for EOS L (dashed curves) and EOS APR (solid curves), and for $\nu = 300$ Hz (light curves) and $\nu = 600$ Hz (heavy curves).

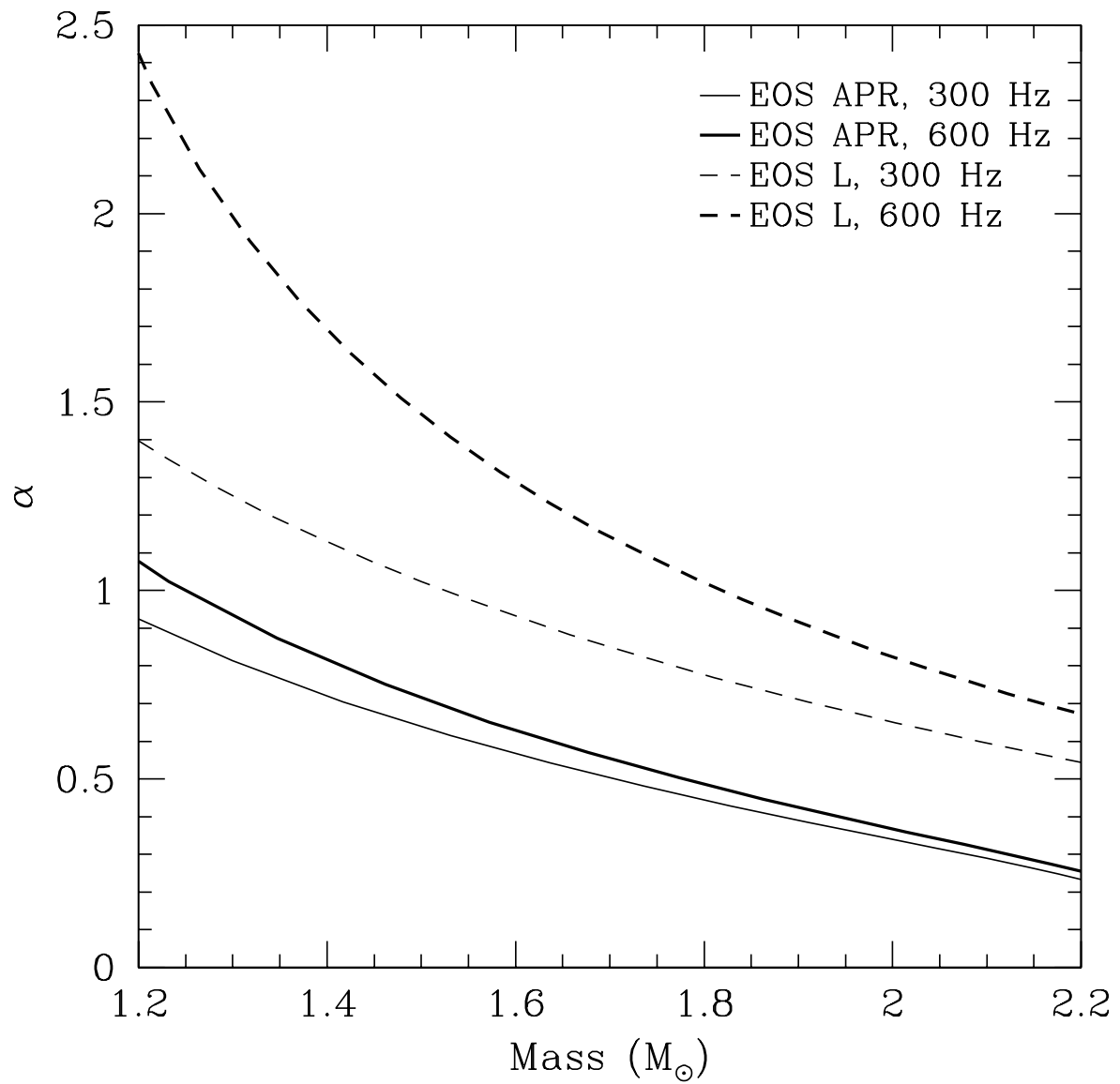


FIG. 3.— The scaling factor α which rescales the fiducial values of $\Delta\Omega/\Omega$ presented in §2 and Figure 1 to different neutron star masses, equations of state, and spin frequencies. The factor α includes the scaling with surface gravity, the correction to gravity at the equator due to rapid rotation, and general relativistic corrections to gravity and the angular momentum conservation law. We show results for EOS L (*dashed curves*) and EOS APR (*solid curves*), and for $\nu = 300$ Hz (*light curves*) and $\nu = 600$ Hz (*heavy curves*).

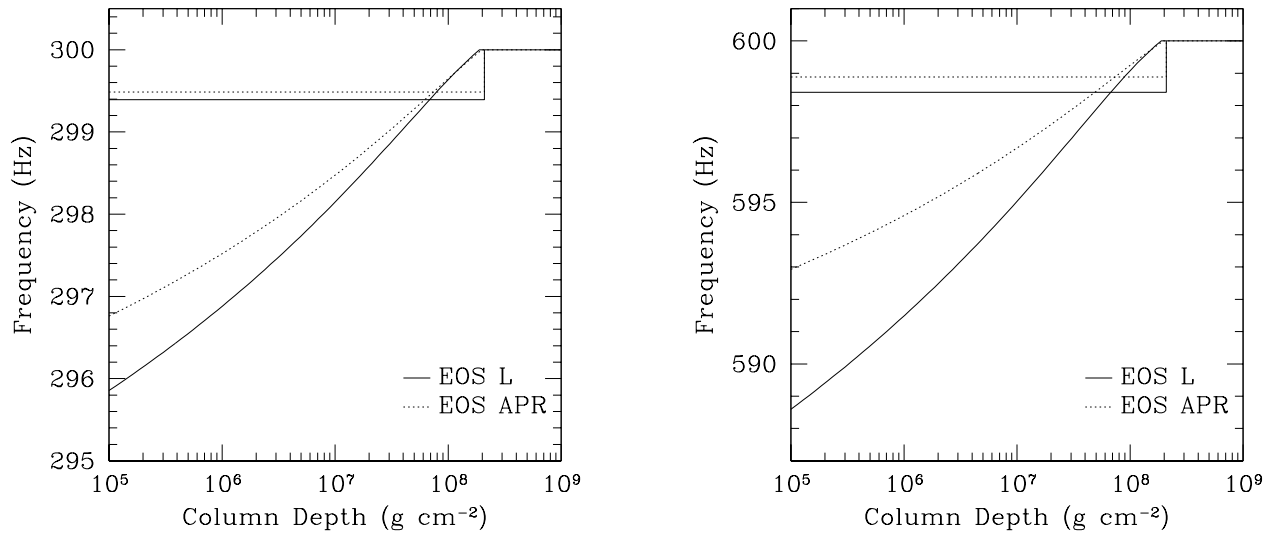


FIG. 4.— Detailed rotational profiles for $1.4 M_{\odot}$ neutron stars undergoing mixed H/He ignition at a global accretion rate of $0.1 \dot{M}_{\text{Edd}}$. We assume that the atmosphere is rigidly-rotating immediately prior to the burst, and that during the burst, the atmosphere is radiative and carries a flux equal to the solar-composition Eddington flux at the photosphere. For $\nu = 300$ Hz (*left panel*) and $\nu = 600$ Hz (*right panel*), and for EOS L (*solid lines*) and EOS APR (*dotted lines*), we plot the rotational profiles assuming either (i) complete rotational coupling, resulting in rigid rotation across the layer, or (ii) no angular momentum transport, giving a differentially-rotating layer.

APPENDIX

ANGULAR MOMENTUM CONSERVATION FOR A FLUID

In this Appendix, we start with the conservation equations for a fluid, which include contributions from the fluid's enthalpy and from heat flow, and show that the appropriate conserved quantity is the angular momentum per baryon u_ϕ as calculated in §3.

We begin with the stress tensor for a fluid

$$T^{\alpha\beta} = h\rho u^\alpha u^\beta + P g^{\alpha\beta} + F^\alpha u^\beta + u^\alpha F^\beta, \quad (\text{A1})$$

(see, for example, Mihalas & Mihalas 1984). The enthalpy h is

$$h = \frac{\epsilon + P}{\rho} \quad (\text{A2})$$

where the energy density

$$\epsilon = \rho c^2 + \rho\Pi - \rho B \quad (\text{A3})$$

is the sum of rest mass energy, internal energy, and nuclear binding energy. We write the heat flux as F^α . By setting $\phi_\beta \nabla_\alpha T^{\alpha\beta} = 0$, and using baryon number conservation $\nabla_\alpha (\rho u^\alpha) = 0$, we obtain the angular momentum conservation law

$$\rho u^\alpha \nabla_\alpha \left(h u_\phi + \frac{F_\phi}{\rho} \right) + \nabla_\alpha (F^\alpha u_\phi) = 0. \quad (\text{A4})$$

Assuming the azimuthal heat flux F^ϕ may be neglected when compared to the vertical heat flux $F^r = F$, we rewrite equation (A4) as

$$\frac{d}{dt} (h u_\phi) = -\frac{1}{\rho} \frac{d}{dz} (F u_\phi). \quad (\text{A5})$$

We now simplify this equation using the first law of thermodynamics, which is

$$d\epsilon = \left(\frac{\epsilon + P}{\rho} \right) d\rho + \rho T ds \quad (\text{A6})$$

where s is the entropy per baryon mass, or, using equation (A2),

$$dh = T ds + \frac{dP}{\rho}. \quad (\text{A7})$$

Substituting for dh/dt in equation (A5), we find

$$\frac{du_\phi}{dt} = -\frac{u_\phi}{h} \left[T \frac{ds}{dt} + \frac{1}{\rho} \frac{dF}{dz} \right] - \frac{u_\phi}{\rho h} \frac{dP}{dt} - \frac{F}{\rho h} \frac{du_\phi}{dz}. \quad (\text{A8})$$

The first term in equation (A8) vanishes, since $T ds/dt = -(1/\rho) dF/dz$ is the familiar entropy equation. The nuclear energy production rate is included in the $T ds/dt$ term, since the nuclear binding energy is included in the enthalpy: equations (A3) and (A6) give

$$T \frac{ds}{dt} = \frac{d\Pi}{dt} - \frac{P}{\rho^2} \frac{d\rho}{dt} - \frac{dB}{dt}, \quad (\text{A9})$$

where dB/dt is the nuclear energy generation rate. Integrating the second term in equation (A8) in time, we find it gives a contribution to $\Delta u_\phi/u_\phi$ of order $\Delta P/\rho c^2 \approx (H/R)(P/\rho c^2) \approx (gR/c^2)(H/R)^2 \approx 10^{-7}$, where we take the pressure scale height $H \approx 10$ m. The third term in equation (A8) represents radiative viscosity (see Mihalas & Mihalas 1984). Again integrating in time, we find that this term gives a contribution $\approx (F/\rho c^2)(t/H)(\Delta u_\phi/u_\phi) \approx 10^{-4}(t/\text{sec})(\Delta u_\phi/u_\phi)$. Both the second and third terms are of order $(H/R)^2$ or smaller, and may be neglected for our purposes.

In summary, consideration of the conservation law for a fluid gives

$$\frac{du_\phi}{dt} = 0 + \mathcal{O} \left(\frac{H}{R} \right)^2, \quad (\text{A10})$$

showing that, at the level of accuracy we require, the angular momentum per baryon u_ϕ is conserved.